AD_____

Award Number: DAMD17-97-1-7030

TITLE: Magnetic Resonance Arterial Spin Tagging for Non-Invasive Pharmacokinetic Analysis of Breast Cancer

PRINCIPAL INVESTIGATOR: Michael Buonocore, M.D.

CONTRACTING ORGANIZATION: University of California, Davis
Davis, California 95616-8671

REPORT DATE: October 1999

TYPE OF REPORT: Annual

PREPARED FOR: U.S. Army Medical Research and Materiel Command
Fort Detrick, Maryland 21702-5012

REPORT DOCUMENTATION PAGE

Form Approved
OMB No. 074-0188

1. AGENCY USE ONLY (Leave blank)	2. REPORT DATE	3. REPORT TYPE AND DATES COVERED
	October 1999	Annual (30 Sep 98 - 29 Sep 99)

4. TITLE AND SUBTITLE
Magnetic Resonance Arterial Spin Tagging for Non-Invasive Pharmacokinetic Analysis of Breast Cancer

5. FUNDING NUMBERS
DAMD17-97-1-7030

6. AUTHOR(S)
Michael Buonocore, M.D.

7. PERFORMING ORGANIZATION NAME(S) AND ADDRESS(ES)
University of California, Davis
Davis, California 95616-8671

e-mail:
mhbuonocore@ucdavis.edu

8. PERFORMING ORGANIZATION REPORT NUMBER

9. SPONSORING / MONITORING AGENCY NAME(S) AND ADDRESS(ES)
U.S. Army Medical Research and Materiel Command
Fort Detrick, Maryland 21702-5012

10. SPONSORING / MONITORING AGENCY REPORT NUMBER

11. SUPPLEMENTARY NOTES

12a. DISTRIBUTION / AVAILABILITY STATEMENT
Approved for public release
distribution unlimited

12b. DISTRIBUTION CODE

13. ABSTRACT *(Maximum 200 Words)*

This research project concerns the development of MRI arterial spin tagging to non-invasively measure breast tissue perfusion. The specific aims are to (1) refine arterial spin tagging pulse sequences, (2) develop automated data analysis software, and (3) compare the technique to first-pass contrast-enhanced MRI and biopsy. The scope of effort is mainly limited to technical developments. However, the project includes a performance comparison with first-pass, contrast-enhanced MRI in 60 patients. During the past year, the spin-tagging pulse sequences have been rewritten for a new, research-only, GE 1.5T Horizon LX Echospeed CV/I MRI system at UC Davis. New image processing software, and software for statistical analysis of spin tagging and contrast enhanced dynamic scans, has been written. Prior software was enhanced for easier use by clinicians. Additional patient studies were not done, due to the loss of the co-investigator on the project, and to the lack of availability of an MRI system that could run the pulse sequences, for several months. As a result, the budget and schedule of the project was officially pushed back approximately six months, into the third year of the project, which was originally designed with very light project activity.

14. SUBJECT TERMS
Breast Cancer, IDEA Award

15. NUMBER OF PAGES
30

16. PRICE CODE

17. SECURITY CLASSIFICATION OF REPORT	18. SECURITY CLASSIFICATION OF THIS PAGE	19. SECURITY CLASSIFICATION OF ABSTRACT	20. LIMITATION OF ABSTRACT
Unclassified	Unclassified	Unclassified	Unlimited

FOREWORD

Opinions, interpretations, conclusions and recommendations are those of the author and are not necessarily endorsed by the U.S. Army.

__✓__ Where copyrighted material is quoted, permission has been obtained to use such material.

_____ Where material from documents designated for limited distribution is quoted, permission has been obtained to use the material.

_____ Citations of commercial organizations and trade names in this report do not constitute an official Department of Army endorsement or approval of the products or services of these organizations.

_____ In conducting research using animals, the investigator(s) adhered to the "Guide for the Care and Use of Laboratory Animals," prepared by the Committee on Care and use of Laboratory Animals of the Institute of Laboratory Resources, national Research Council (NIH Publication No. 86-23, Revised 1985).

__✓__ For the protection of human subjects, the investigator(s) adhered to policies of applicable Federal Law 45 CFR 46.

_____ In conducting research utilizing recombinant DNA technology, the investigator(s) adhered to current guidelines promulgated by the National Institutes of Health.

_____ In the conduct of research utilizing recombinant DNA, the investigator(s) adhered to the NIH Guidelines for Research Involving Recombinant DNA Molecules.

_____ In the conduct of research involving hazardous organisms, the investigator(s) adhered to the CDC-NIH Guide for Biosafety in Microbiological and Biomedical Laboratories.

Herbert H Bunocore 10/28/99

PI - Signature Date

Table of Contents

Introduction

This research project concerns the development of MRI arterial spin tagging to non-invasively measure breast tissue perfusion. MR dynamic first-pass contrast-enhanced imaging has shown that malignant and benign breast lesions can be distinguished. However, it may have limited importance in clinical breast diagnosis due to significant false-negatives and false-positives. The arterial spin tagging technique was developed to measure tissue perfusion parameters without the use of contrast, and has been successfully demonstrated in brain and kidney. The specific aims are to (1) refine arterial spin tagging pulse sequences and imaging protocols, (2) develop automated data analysis software for measurement of breast tissue parameters, and (3) compare the technique to first-pass contrast-enhanced MRI and biopsy. We will test the hypothesis that arterial spin tagging provides accurate and precise discrimination between normal tissue, benign and malignant lesions, when differences in perfusion and T_1 exist. Lesions will have been previously detected by clinically accepted diagnostic imaging procedures, and by biopsy. Statistical analysis will be performed to access the correspondence between arterial spin-tagging and biopsy, and to establish the relative value of spin tagging compared to first-pass contrast-enhanced MRI. We hope to establish that, relative to using first-pass contrast-enhanced imaging, false positives and negatives are reduced using arterial spin tagging by virtue of increased image signal-to-noise ratio (SNR), higher spatial resolution, and the unique ability to obtain estimates of macromolecular bound fluid fractions. The scope of effort on the project is mainly limited to the technical aspects of development of a new methodology. However, the project also includes a rigorous performance comparison with the current gold-standard methodology. The technique will be evaluated in sixty patients, with roughly equal numbers of benign and malignant lesions.

Body

Description and Chronology of Project Schedule Changes

Summary of Project delays

The major deficiency in our progress is with the third technical objective. Specifically, comparison of the arterial spin tagging sequence with the dynamic contrast enhanced first pass study has not yet been achieved. Roughly 60 patients should have been scanned at this point in the project, but only two have been scanned. This deficit is due to the delay in finding a replacement physician for the co-I on the project, Rebecca Zulim, who left UCDMC November 1, 1998. Also, UCD Medical Center Radiology Department upgraded all their MRI systems from Signa Genesis 5.x to Signa LX 8.2.5, resulting in several months during which our pulse sequences were not compatible with any of the MRI systems we had access to. Substantial time was needed to convert the pulse sequences to the LX 8.2.5 platform from the Genesis 5.x platform. This time period for upgrading the UCD Med Center MRI systems was not planned in advance, and the time to convert our research software was not written into the approved Work Statement. The graduate student on this project, David Zhu, and I have worked on the conversion of the arterial spin tagging pulse sequences, and on the development of new arterial spin tagging sequences based on our "odd-hybrid" EPI technique [Buonocore MH, Zhu DC. High spatial resolution EPI using an odd number of interleaves. Magnetic Resonance in Medicine 41 (6): 1199-1205 (1999)]. Also, advances have been made in our image processing software for the project. Because of the delays, the budget and schedule was officially pushed back 6 months, into the 3rd year which had a light work schedule. For full details, please see the referenced letter dated April 20, 1999, and the approved Budget change, in the appendix material. The project now continues into the 3rd year, as dictated by approved revised schedule and budget. Dr. PD Schneider is the co-investigator on the project.

Project timeline changes

Rearrangement of budget and project schedule

April 1999: With the realization that original co-Investigator Rebecca Zulim, MD, having moved to Kaiser Permanente, was no longer going to be effective as co-investigator on this project, I submitted, on April 20, 1999, a long letter explaining the situation, along with a revised budget to the US Army-BCRP office. Because the work schedule in the third year was relatively light, I requested transfer of remaining salary support and unexpended funds from the 2nd year, to the third year starting Oct 1, 1999. Over half of the salary support was unexpended (March 1999 through October 1999 salary was transferred). Supplies costs were also carried forward. The stipend and tuition remission of the graduate assistant, David Zhu, could not be deferred. He continued to work toward the specific aims of the project throughout the project period. The letter dated April 20, 1999, and the approved Budget change, are included in the appendix material of this Report.

May 1999: The revised budget and schedule is approved by the US Army BCRP.

Major events in Co-Investigator change

Nov 1, 1998: Rebecca Zulim quits UCD Medical Center, and begins work at Kaiser Permanente in Sacramento. There is no replacement for her at UCD Medical Center. Rebecca did not inform me of her intent to leave UCD. Apparently, the Surgical Oncology

Department was not aware of it either, since there was no recruitment effort in place at that time. At this point, I had no physician on the project to recruit patients.

December 1999: Rebecca expresses interest in continuing the research collaboration while she is at Kaiser. As PI, I rewrite the Protocols and Consent Form for recruitment of patients at Kaiser, and submit these to our Human Subjects Review Committee (HSRC). Rebecca submits same protocol and consent to the Kaiser HSRC.

March 1999: There is still no response from the Kaiser HSRC. Rebecca continues to say that she wants to collaborate, but it is becoming more clear that it will not work out. I received the UC Davis HSRC committee action on the revised Protocol and Consent Form that I submitted in order to recruit patients from Kaiser. The UC Davis HSRC committee requires minor corrections for approval of the protocol, but I do not submit these corrections, due to the non-responsiveness of Kaiser's HSRC.

April 1999: I contact Phil Schneider, MD-PhD, Director of the Surgical Oncology at UCD Medical Center, to let him know that Rebecca is not going to collaborate at Kaiser. I request his participation, or that of a clinical fellow. He agrees to collaborate, and I rewrite the Protocol and Consent Form a second time to revert back to patient recruitment at the UCDMC Oncology Clinic, and to include him as collaborator.

May 24, 1999: the UC Davis HSCR approves the modified protocol and consent, reestablishing our intent to recruit from UC Davis Clinics. The only modification from the original approved consent is the inclusion of Dr. Schneider (and removal of Dr. Zulim). I also prepared a advertising flyer which is included in the revised consent.

July 1999-Oct 1999: Patients are not being recruited, due, according to Dr. Schneider, to his preoccupation with other projects. However, he reconfirms his commitment to the project and suggests that I visit the clinic each week to post the flyer.

Major events in MRI system upgrades

December 1998: The main hospital MRI is upgraded to Horizon LX Echospeed, Version 8.2, from Signa Advantage OS Version 5.4. This invalidates our pulse sequence software. Because the Imaging Center MRI is not yet available for research use, there is no system at UC Davis on which patient studies can be done.

December 17, 1998: Purchase order is placed with GE for upgrade of the MRI Signa Advantage System at the UCD Imaging Center to a high-performance CV/i system. The intent of the Radiology Dept. is to convert this system into one dedicated to MRI research The Radiology Department Chair designates the Imaging Center system as the official MRI Research System. All Breast Imaging Studies are to be done at this site, as soon as the system is delivered.

December 1998-April 1999: The graduate student and I spend our time on the project learning the EPIC pulse sequence for LX environment, obtaining relevant source codes and programs for conversion of research pulse sequences. Acquisition of the EPIC 8.2.5 compilers from GE was delayed due to our research agreement negotiations, which were completed in May 1999. We currently have a five-year agreement starting May 1, 1999. Acquisition of the EPIC software was also delayed due to GE administrative delays. For example, the EPIC compilers for Version 8.2.5 were not obtained until issues regarding the long-term research agreement were resolved

April 1999: Research MRI is installed at the Imaging Center. Work begins on conversion of pulse sequences. Significant performance problems with the system delay getting the software converted and running properly for use in patients. Full payment for the system is

not made. 90% of payment made in July 1999, remaining 10% to be made in November, 1999, with stipulations.

April 1999-Sept 1999: The arterial spin tagging breast sequence based is converted from Version 5.4 to 8.2.5, and uses the enhanced gradients of the CV/I high performance system. In addition, the odd-number interleaf EPI sequence (see appendix for copy of this publication) is converted. Current work involves incorporating this acquisition into the arterial spin tagging sequence. In other words, instead of SPGR acquisition with short TR, there is EPI acquisition. We test both the "odd-number interleaf" EPI sequence, and the even-number interleaf sequences that GE provided through the UC Davis Research Agreement. For full details, see section below on pulse sequence development.

Discussion of Approved Statement of Work

Technical objective 1

Task 1*: Months 1-6: Implementation and testing of magnetization transfer pulses for both arterial tagging and first-pass contrast enhanced sequences.*

Report for 1999

Magnetization transfer (MT) has been implemented with the EPI-based spin tagging sequence (see Figure 1). The MT radiofrequency (RF) pulse selectively excites the protons of the macromolecules and its hydration layer by a 90^0 flip angle. Two gradient spoiling pulses (in the x- and y- directions) are applied immediately after the RF pulse to spoil the transverse magnetization. The usual RF excitation pulse for data acquisition is applied immediately after these spoiling pulses. Due to hardware and or compiler problems that are currently being investigated by GE, this pulse sequence has been implemented only on pulse sequence simulation software (EPIC), not yet on the MRI system. The hardware problems are somehow preventing this sequence from running successfully on the MRI system. Testing of MT using the fast SPGR-based sequence revealed that it would not be effective. Because the magnetization transfer RF pulse is long duration (16 ms), the "small TR" (*optr*) period of the fast SPGR sequence was effectively doubled in length, thus sacrificing short scan time and distorting the signal upon which the perfusion measurement is based.

From 1998 Annual Report …

Magnetization transfer pulses have not been implemented yet. Mainly, this delay was due to the fact that the MRI system at UC Davis Medical Center is scheduled to be upgraded to the new Horizon LX system soon, and we opted to defer this pulse sequence development until we were using this new LX software platform. There have been multiple delays, but this upgrade is scheduled to occur by January 1999. The existing pulse sequence will be converted from the 5.4 OS platform to the LX2 platform (a substantial change), and the magnetization transfer pulses will be implemented also.

Because of concerns regarding the ultimate utility of the magnetization transfer technique, we have decided that implementation and testing of arterial spin-tagging sequence based on echo planar imaging (EPI) data acquisition is a higher priority. EPI based spin-tagging technique can theoretically improve the accuracy of the T_1 estimation, which we have studied and worked with extensively (see below). The major problem with magnetization transfer is that it represents a perturbation on an already small signal. Therefore, whether we will observe a magnetization transfer effect is questionable. Nevertheless, it will be implemented as part of the project.

Task 2*: Months 1-9: Implementation and testing of interleaved high-resolution imaging technique, for both arterial tagging and first-pass contrast enhanced sequences.*

Report for 1999

Summary

Since the completion of the upgrade of the UC Davis Imaging Center MRI system, and since it's designation as *the* Research MRI system for UC Davis, we have thoroughly studied the EPIC LX 8.2.5 programming language for pulse sequence development, and the operation of this new MRI system. The transition to the new research MRI required a complete rewrite of all pulse sequence software that we had developed for this project. In addition, we revised the pulse sequences to utilize the high performance gradients (40 mT/m peak, 150 mT/m/ms rise) of the system. We believe these revised sequences will provide much better arterial spin tagged data for perfusion measurement. All of the other sequences in our breast imaging protocol were set up for the new LX 8.2.5 platform as well.

Conversion of the Fast SPGR Based Arterial Spin Tagging Sequence

The authors converted the fast SPGR-based arterial spin tagging pulse sequence from the Genesis 5.4 platform to the LX 8.2.5 platform. The converted sequence was also improved to achieve higher resolution with a shorter overall scan time. The new MR system has higher peak gradient amplitude and slew rate. Fast data acquisition, which requires the higher read-out gradient amplitude (4.0 g/cm) could be specified, and consequently the data acquisition period (*optr*) was shorten from 16.62 ms to 12.5 ms. Since *optr* was shortened, a larger matrix in the phase encode direction could be specified. The resolution is now 256 × 256 matrix using a one-half phase field of view acquisition. Previously we used a 256 × 240 matrix with one-half phase field of view acquisition. The total time for the image acquisition (the TR period), including the global inversion RF pulse, has been decreased from 2.7 seconds to 2.22 seconds. The performance of this new sequence has been confirmed using phantoms and one test subject.

Development of an EPI-Based Arterial Spin Tagging Sequence

The EPI-based arterial spin tagging sequence was rewritten and verified on the research MRI system. The data acquisition scheme is based on our recently published high-resolution odd-number interleaf EPI sequence [Buonocore MH, Zhu DC. High spatial resolution EPI using an odd number of interleaves. Magnetic Resonance in Medicine 41 (6): 1199-1205 (1999)]. This sequence was first developed and verified on the Signa Advantage 1.5 T GE MR system. Unfortunately, under the new LX system, the polarity alternation scheme for each successive interleaf we had implemented caused the system to hang, and substantial time was expended understanding the problem. In October 1999, we formulated an alternative approach to eliminate the requirement of polarity alternation, which was successfully implemented. One persistent problem that we have with all interleaved EPI sequences on the LX system, is reduced SNR relative to theoretical predictions. The cause of this is not known.

In the new arterial spin tagging sequence using the interleaved EPI acquisition, the following steps are performed at each interleaf: (1) non-selective RF inversion pulse, (2) 20 EPI acquisitions, each of which is preceded by a 10^0 RF pulse (Figure 2). These 20 acquisitions are played out with a repetition time (*optr* in Figure 2) of 100 ms. Each acquisition defines one point on a T_1 recovery curve. The total time for each interleaf (*TR* in Figure 5.10) is 2 seconds. Data for the other interleaves is collected in the same fashion in subsequent TR intervals. Figure 3 shows the loop nesting. The completed set of images, showing T1 recovery of the magnetization, is acquired in two seconds times the number of interleaves.

From 1998 Annual Report ...

An interleaved arterial spin-tagging technique, that allows high resolution (e.g. 256 x 256 or more) has been implemented and tested. We also implemented a rectangular data acquisition technique, which acquires data sets that have different numbers of points along the frequency and phase encode direction. The 256 x 240 interleaved acquisition provides the best spatial versus temporal resolution tradeoff, and has been used for all of our recent studies.

Task 3*: Months 1-9: Analysis of spin tagging sequence to understand causes of existing baseline offsets, effects of inversion slice transition profiles, and effects of RF flip angle profile on the measurements, with implementation and testing pulse sequence modifications to minimize these imperfections.*

Report for 1999

Regarding the spin tagging sequence utilizing fast SPGR, these issues were treated in the 1998 report. The EPI arterial spin tagging sequence has not been evaluated, but the same solutions for the inversion slice transition profiles, and effects of RF flip angle profile, will apply.

From 1998 Annual Report ...

Matching of inversion and excitation slice profiles was greatly improved by using customized RF pulses designed with the Shinnar-Le Roux (SLR) algorithm. The new data processing technique (based on a semi-log linear regression of inversion time (TI) dependent signal) significantly reduced the previously reported problem in measuring the longitudinal relaxation time (T1) caused by baseline offsets, and by the uncertainty in the effective inversion time. The optimal RF flip angle for spin excitation during spatial encoding was found to be 10 degrees, based on experiments over a range of flip angles.

Technical objective 2

Task 4*: Months 3-15: Software for automatic estimation and error analysis of perfusion, tissue water longitudinal relaxation time, and extracellular fluid volume fraction from mathematical models and user-defined ROIs from spin tagging timeseries. Implementation of pharmacokinetic model calculations and error analysis for first-pass contrast enhanced imaging.*

Report for 1999

From October 1998 through April 1999 (during which time there was no MRI system for us to develop on, or do patient studies), image processing software development continued. Improvements in the BreastView program, development of "dispAlls" program for analysis of general MRI images, and implementation of statistical analysis of breast lesions based on Bayesian approach, was completed. Statistical analysis of available breast lesion data continued (See below). The most important new function of BreastView is that for analysis of the first-pass contrast enhanced images. The program creates an image based upon the time derivative of the rate of rise of the signal, so that the contrast enhancement effect can be better visualized (See Figures 4 and 5).

From 1998 Annual Report ...

A software program (BrView) has been written in C, X Window System, and Motif, and implemented on an SGI O2 computer (paid for by grant funds) for

analyzing and visualizing the MR images and timeseries. Much effort has been expended on developing the capability to easily review all of the images taken in each study, and cross-reference pixel locations. Much more effort than anticipated has been expended in the development of a robust technique for identifying so-called "suspicious regions" based on the T_1 and perfusion measurements. The measurement of T_1, upon which the perfusion measurement entirely depends, is based on a semi-log linear regression technique developed by the investigators. The T_1, perfusion (f/λ) and standard errors of these quantities are estimated automatically using this robust technique. The so-called feature images display these quantities in color and grayscale. These quantities are used to calculate a "suspicion index" for each pixel, and thereby identify regions of breast tissue suspicious for malignancy.

The implementation of the pharmacokinetic model calculations and error analysis for first-pass contrast enhanced imaging has not been completed. Thus far, the software allows the user to click on the reference image of the dynamic study, to display the time profile of the signal at that pixel. The implementation of the pharmacokinetic model is currently a major focus of the current effort.

Task 5*: Months 3-15: Software for registration (including implementation and testing of motion correction and physiological noise reduction algorithms) and overlay of images from high resolution* T_1 *weighted, spin-tagging, and contrast enhanced studies.*

Report for 1999

First described in the 1998 Annual Report, the BreastView program has been continually upgraded and enhanced with the latest algorithms for processing and analysis of breast imaging studies, including those for spin-tagged and dynamic contrast enhanced images. The specific developments this year of BreastView, and of another program, dispAlls, are described.

BreastView

Between October 1998 and April 1999, the BreastView program was made "clinician-friendly". The graphical user interface now guides the user through the entire visualization and analysis process for a breast imaging study. A "Help" button, linked to extensive set of manual pages, now appears on the first page of the interface. Clicking the Help button brings up an html file with necessary operating instructions. The help files were written for clinicians. The clinician can now begin using the program without first studying the written instructions. If an inappropriate option is selected, the program now provides help to the user to select a more appropriate option or operation. Several new features and functions have been implemented, as indicated on Figures 6 and 7. The most important new function of BreastView is the analysis of the first-pass contrast enhanced images. The program creates a contrast enhancement-weighted image based upon the time derivative of the rate of rise of the signal, so that the contrast effect can be better visualized (See Figures 4 and 5).

The dispAlls program

This program has been written for quickly viewing and performing ROI analysis on one or a series of images. The program is particularly useful for quickly reviewing the timeseries of signal changes in an ROI from the dynamic contrast enhanced studies. The program displays one image, or a sequence of images, with or without an image header. It performs ROI analysis and plots the calculated values.

From 1998 Annual Report ...

Using the BrView software program, image pixels containing high values of perfusion (f/λ), and moderate to high values of T_1, and low standard errors, are identified as suspicious, and assigned a "suspicion index" based on finding similar abnormal values at spatially adjacent pixels. Suspicious pixels can be overlaid on the high-resolution T_1 and T_2 clinical images by color mapping, and simultaneously presented with the first-pass contrast enhanced timeseries at these pixels. This provides the user with a comprehensive anatomical and functional view of the suspicious regions, and facilitates making a decision regarding the malignant nature of the lesion. Finally, a motion artifact estimation and correction algorithm has been developed and implemented in a separate software program.

Technical objective 3

Task 6: *Months 9-24: 60 patients with malignant and benign breast lesions will be imaged using* T_1 *weighted, first-pass contrast enhanced, and arterial spin tagging MRI pulse sequences.*

Report for 1999

Unfortunately, no additional subjects have been done. This is due to the loss of Rebecca Zulim, MD, as the co-investigator, and the transition to a dedicated research MRI system that operated at LX 8.2.5, as described above. Through Sept 1998, eighteen subjects, including 11 patients referred by their physicians and seven volunteers referred by themselves, had participated in the breast studies. Three patients and two volunteers were eliminated from the analysis because the studies were not done according to protocol, due to excess motion, or the abnormal mass being too close to the chest wall to be measured reliably, or no patient biopsy to confirm the MR study result. There are total of 13 useful cases left for analysis. For all these cases, the suspicious pixels were identified based on the following criteria: T_{1n}: > 0.5 sec f/λ: > 0.1 sec^{-1}, STD of f/λ: < 0.1 sec^{-1}, and the suspicion level threshold was set at 20.2%. Analysis has been done using the program BreastView. Table 8.5 shows the result of these 13 cases.

Table 8.5. Summary of Breast Case Studies

Date of Study	Subject Referred by	Palpable (Yes or No) ?	Seen on Clinical MRI ?	Level of Suspicion Based on T_{1n} and f/λ	Assessment Based on Suspicion Level	Abnormal Mass Type
05/03/97	Physician	No	Yes	Low	Negative	Benign (Fibroadenoma)
05/23/97	Physician	Yes	Indeter-minable	Moderate High	Positive	Malignant (Ductal Carcinoma)
08/01/97	Physician	Yes	No	High	Positive	Malignant (Ductal Carcinoma)
11/15/97	Physician	Yes	No	Low	Negative	Benign
12/10/97	Physician	Yes	No	High	Positive	Benign

04/13/98 Physician	Yes	Indeter-minate	Moderate High	Positive	Benign
07/27/98 Physician	Yes	No	Low	Negative	Benign
08/07/98 Physician	Yes	No	High	Positive	Benign
02/07/97 Self	No	No	Low	Negative	Normal
03/05/97 Self	Yes	Yes	Low	Negative	Benign (Fibroadenoma)
07/26/97 Self	No	No	Low	Negative	Normal
11/16/97 Self	Yes	Yes	Low	Negative	Benign (Fibroadenoma)
12/14/97 Self	No	No	Low	Negative	Normal

Normal = normal subject who does not have any tumor based on reliable health history, Abnormal Mass Type = determined based on biopsy or reliable health history. Based on the summary shown in Table 8.5, the number of true positive (TP) is 2; the number of false negative (FN) is 0; the number of false positive (FP) is 3 and the number of true negative (TN) is 8. Therefore, the true-positive fraction or sensitivity is 100%, calculated by TP/(TP+FN). The false-positive fraction is 27.3%, calculated as FP/(FP+TN). The specificity is 72.7%, which is equal to one minus the false-positive fraction. Because the number of cases investigated is small, these figures do not provide sufficient statistical confidence to evaluate the technique. After more breast cases have been completed, a ROC curve can be generated using different suspicion level thresholds or different thresholds of T_{1n}, f/λ and STD of f/λ. If a large pool of case studies is available, a more sophisticated Bayesian statistical model can also be generated.

From 1998 Annual Report ...

We have recruited only two subject studies for both first-pass contrast enhanced and arterial spin tagging MRI pulse sequences. Now that the software development is substantially completed, we are trying to improve the rate at which patients are recruited into the study. It is likely that the patient studies will extend into the third year of the proposal. We are currently discussing with physicians at a local Kaiser Hospital for recruitment of additional patients. Appropriate documentation will be submitted for approvals upon reaching a firm agreement.

Task 7 (listed as Task 6 in the original grant application): *Months 12-36: Automated pharmacokinetic analysis, blinded image reading, and statistical comparison of arterial spin tagging, contrast enhanced MRI, and biopsy results.*

Report for 1999

We developed an analysis program for the detection of the features of the dynamic contrast enhanced study, and have developed a statistical approach to the determination of the malignant status of the lesion.

Bayesian Statistical Analysis

The identification of a suspicious pixel based upon the index threshold, that was developed last year, is a simple approach to cancer detection. When a large number of studies becomes available, a Bayesian decision technique [53] will be applied. This technique will be used to

provide ROC (receiver operating characteristic) curves that are commonly used for evaluation of diagnostic algorithms. To summarize the Bayesian technique, let vector space $\mathbf{x} = (T_1, f/\lambda$, STD of f/λ, etc.) for a ROI (region of interest) in a breast. The risks associated with a given vector $\mathbf{x}$ are

$$\text{Risk(Label Benign} \mid \mathbf{x}) = r(\text{Label Benign} \mid \text{Malignant})\, P(\text{Malignant} \mid \mathbf{x}) + r(\text{Label Benign} \mid \text{Benign})\, P(\text{Benign} \mid \mathbf{x}) \tag{7.1}$$

and

$$\text{Risk(Label Malignant} \mid \mathbf{x}) = r(\text{Label Malignant} \mid \text{Malignant})\, P(\text{Malignant} \mid \mathbf{x}) + r(\text{Label Malignant} \mid \text{Benign})\, P(\text{Benign} \mid \mathbf{x}) \tag{7.2}$$

where, Risk(Label Benign | $\mathbf{x}$) = the risk value to label a ROI "Benign" for a given $\mathbf{x}$, Risk(Label Malignant | $\mathbf{x}$) = the risk value to label a ROI "Malignant" for a given $\mathbf{x}$, r(Label Benign | Malignant) = the risk factor to label a ROI "Benign" but actually be malignant, r(Label Benign | Benign) = the risk factor to label a ROI "Benign" and actually be benign, r(Label Malignant | Malignant) = the risk factor to label a ROI "Malignant" and actually be malignant, r(Label Malignant | Benign) = the risk factor to label a ROI "Malignant" but actually be benign, P(Malignant | $\mathbf{x}$) = the probability of being malignant for a given $\mathbf{x}$, and P(Benign | $\mathbf{x}$) = the probability of being benign for a given $\mathbf{x}$. Generally, there is no risk for correct labeling, and thus r(Label Benign | Benign) = 0, and r(Label Malignant | Malignant) = 0. Eq. (7.1) and (7.2) then become

$$\text{Risk(Label Benign} \mid \mathbf{x}) = r(\text{Label Benign} \mid \text{Malignant})\, P(\text{Malignant} \mid \mathbf{x}) \tag{7.3}$$

and

$$\text{Risk(Label Malignant} \mid \mathbf{x}) = r(\text{Label Malignant} \mid \text{Benign})\, P(\text{Benign} \mid \mathbf{x}) \tag{7.4}$$

Furthermore, since,

$$P(\text{Malignant}|\mathbf{x}) = \frac{p(\mathbf{x}|\text{Malignant})P(\text{Malignant})}{p(\mathbf{x})} \tag{7.5}$$

and

$$P(\text{Benign}|\mathbf{x}) = \frac{p(\mathbf{x}|\text{Benign})P(\text{Benign})}{p(\mathbf{x})} \tag{7.6}$$

we have

$$\begin{aligned} \text{Risk Ratio} &= \frac{\text{Risk(Label Benign} \mid \mathbf{x})}{\text{Risk(Label Malignant} \mid \mathbf{x})} \\ &= \frac{r(\text{Label Benign} \mid \text{Malignant})\, P(\text{Malignant} \mid \mathbf{x})}{r(\text{Label Malignant} \mid \text{Benign})\, P(\text{Benign} \mid \mathbf{x})} \\ &= \frac{r(\text{Label Benign} \mid \text{Malignant})}{r(\text{Label Malignant} \mid \text{Benign})} \frac{p(\mathbf{x} \mid \text{Malignant})}{p(\mathbf{x} \mid \text{Benign})} \frac{P(\text{Malignant})}{P(\text{Benign})} \end{aligned} \tag{7.7}$$

The ratio $\frac{\text{r(Label Benign | Malignant)}}{\text{r(Label Malignant | Benign)}}$ is estimated by the clinician. The ratio $\frac{\text{p(x | Malignant)}}{\text{p(x | Benign)}}$ is determined from a training data set. The ratio $\frac{\text{P(Malignant)}}{\text{P(Benign)}}$ can be obtained from literature or estimated from the training data set; but the source of the ratio obtained must correspond with the source of subjects used in the breast study. If the Risk Ratio is greater than 1, then the ROI would be labeled "Malignant"; otherwise, the ROI would be labeled "Benign". Or

$$\text{Risk Ratio} \begin{array}{c} \text{Label Malignant} \\ > \\ < \\ \text{Label Benign} \end{array} 1 \qquad (7.8)$$

The values of risk factors are determined by the clinician or the researcher based on his/her experience. For example, if the clinician thinks that it is too risky to label a malignant mass to be "Benign", he/she would give a high value for r(Label Benign | Malignant), and a relative low value for r(Label Malignant | Benign). Choosing the different values of the risk factor ratio $\frac{\text{r(Label Benign | Malignant)}}{\text{r(Label Malignant | Benign)}}$ is equivalent to choosing different values of the decision threshold. The pairs of false positive and true positive fractions resulting from the different values of the risk factor ratio would allow the plotting of the ROC curve, which can be used to evaluate the performance of the technique presented [1].

The two ratios, $\frac{\text{p(x | Malignant)}}{\text{p(x | Benign)}}$ and $\frac{\text{P(Malignant)}}{\text{P(Benign)}}$, requires a large training data set to be statistically significant. This requires more breast case studies in the future.

Figures

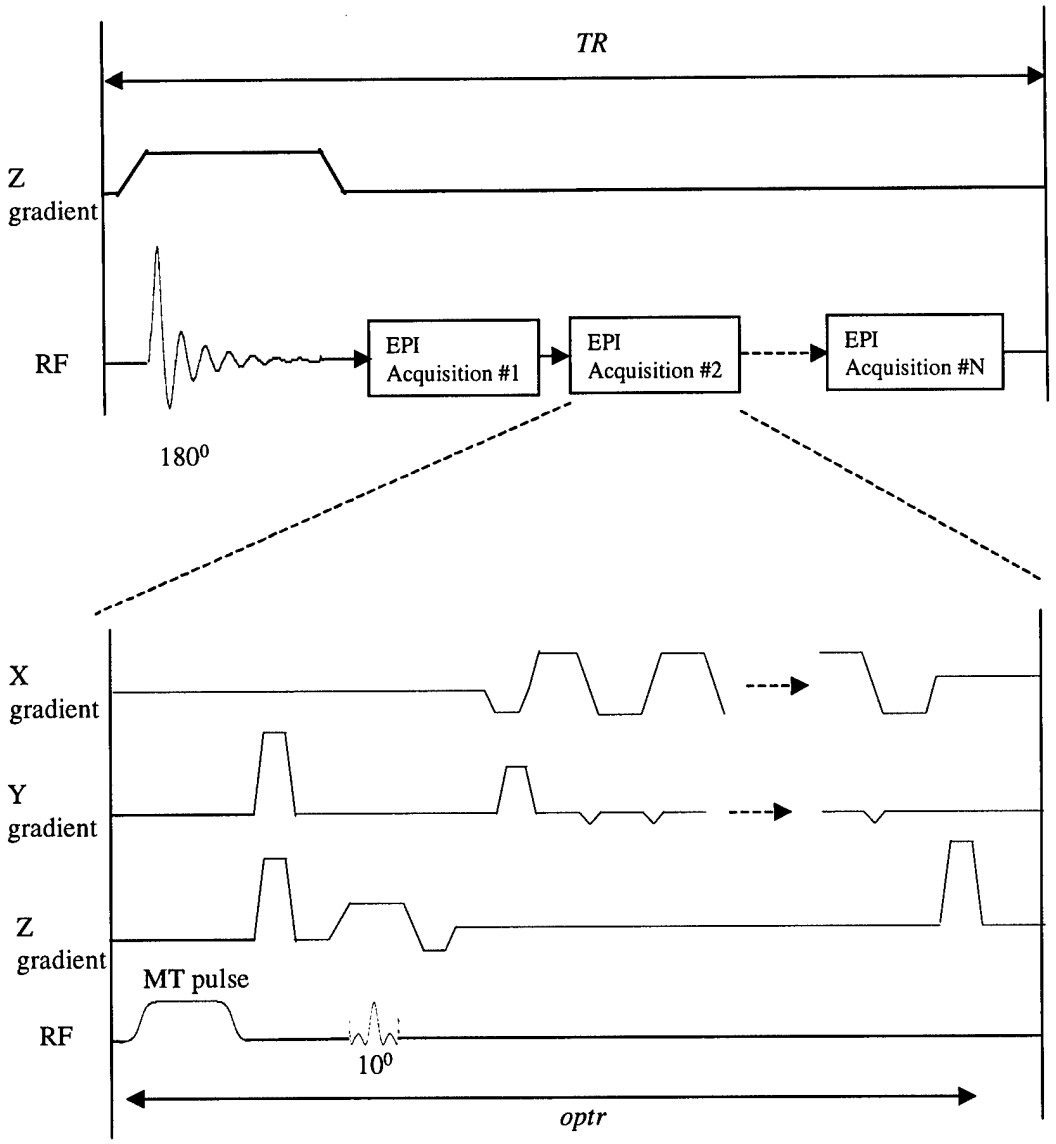

Figure 1. The EPI based spin tagging sequence with MT pulses incorporated. The odd-number interleave EPI technique discussed is implemented in data acquisition. The upper figure shows the timing diagram for each interleave at acquisition. A 180^0 degree RF pulse is followed by N repeated EPI data acquisitions (as shown at the lower figure).

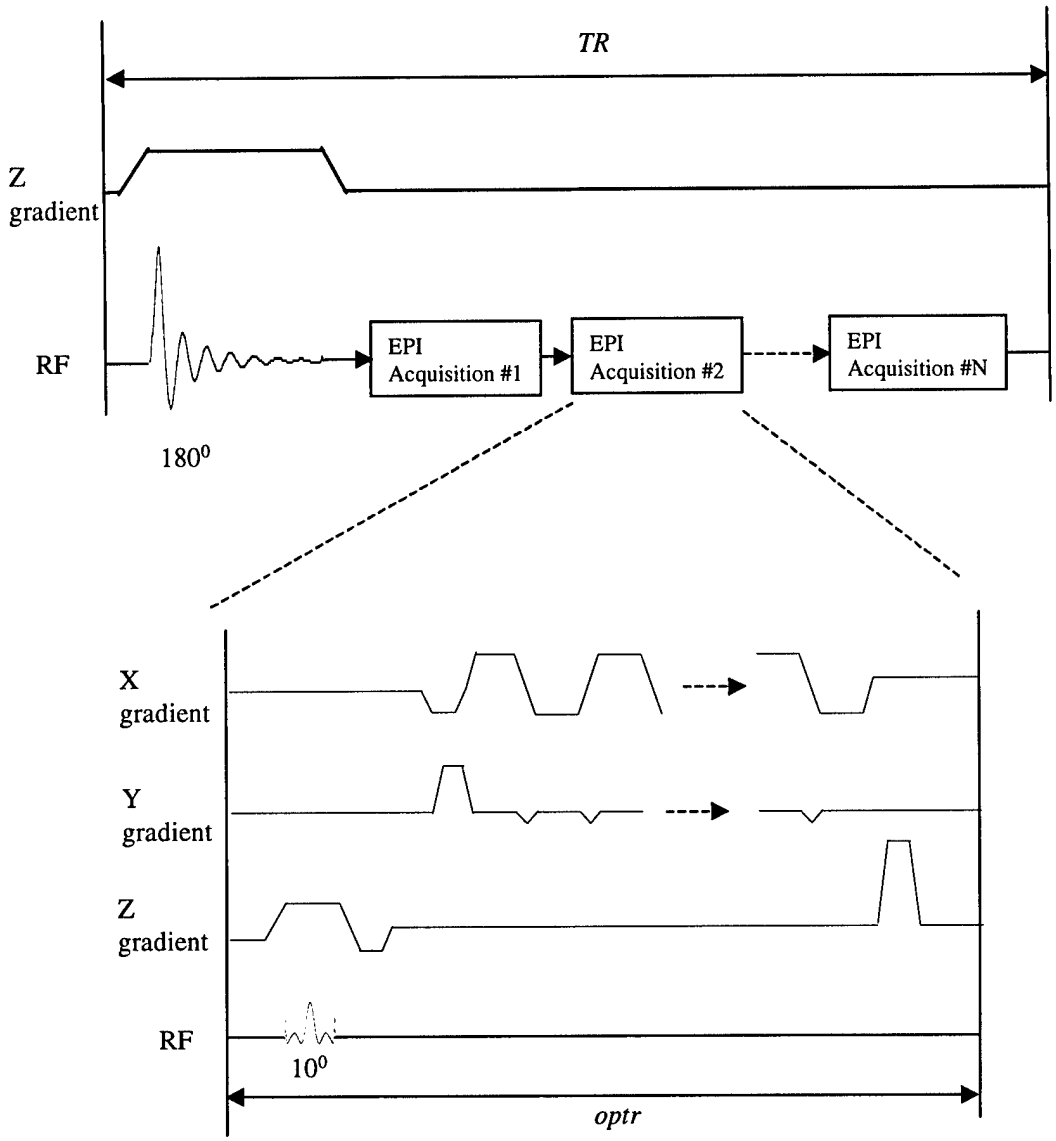

Figure 2. The EPI based spin tagging sequence. The odd-number interleave EPI technique discussed is implemented in data acquisition. The upper figure shows the timing diagram for each interleave acquisition. An 180^0 degree RF pulse is followed by N repeated EPI data acquisitions (as shown in the lower figure).

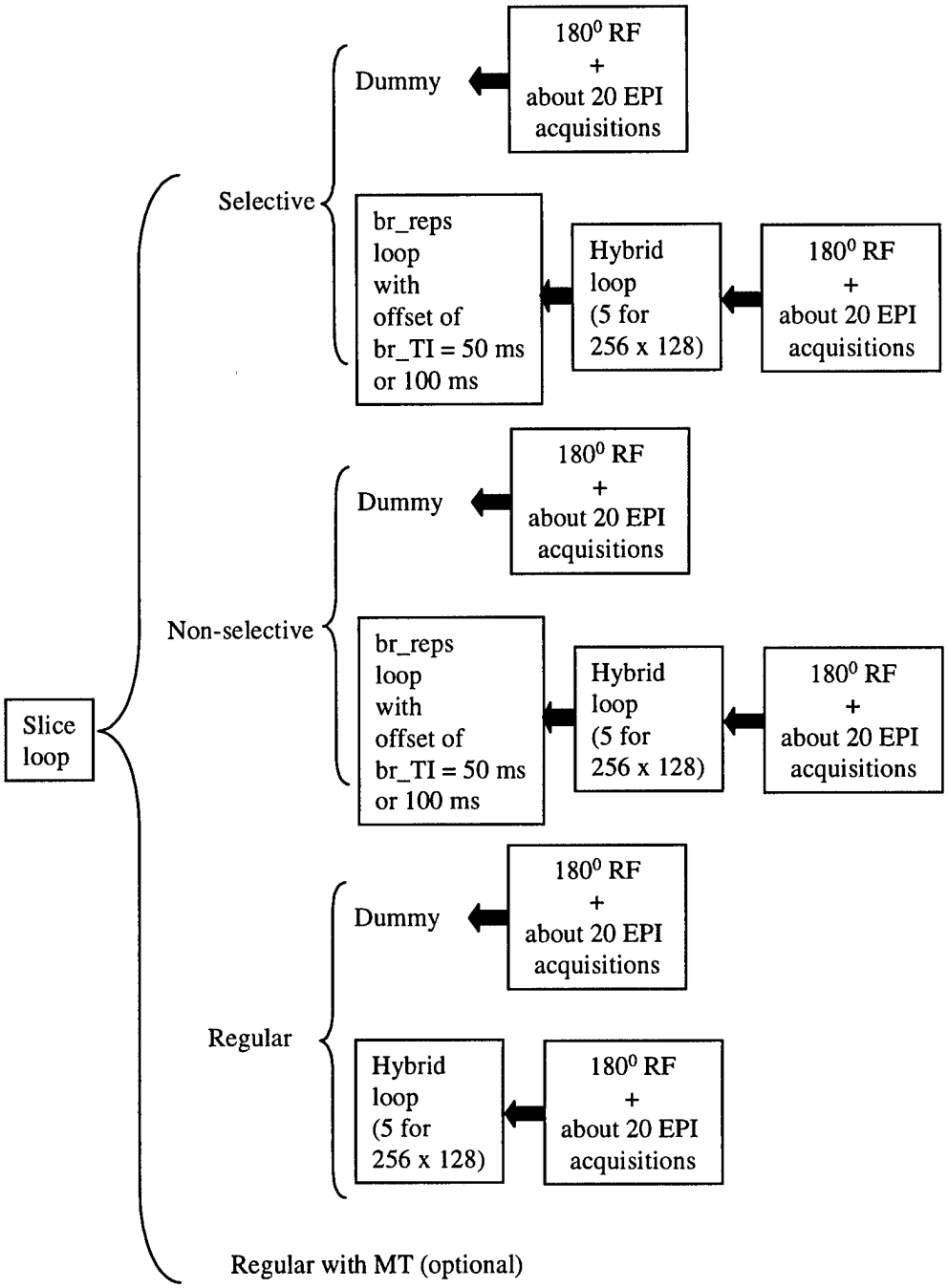

Figure 3. The loop nesting for the EPI based spin tagging sequence.

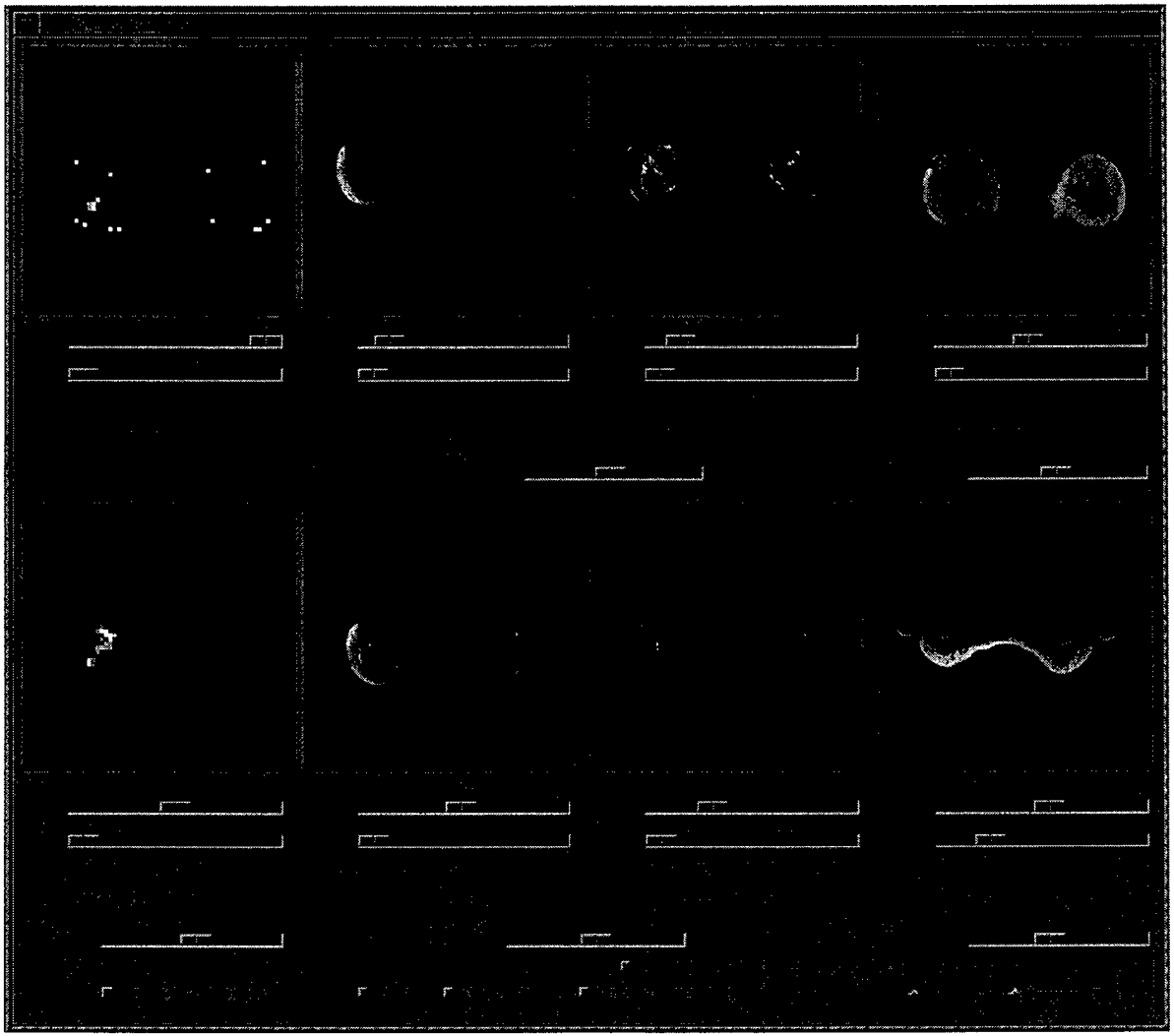

Figure 4. Aug 7, 1998 breast study. Figure shows the T_1 image (1st from left), pre-contrast 3D image (2nd from left), post-contrast 3D image, last image of dynamic study, suspicion map, proton density, T_2 and axial T_1 images.

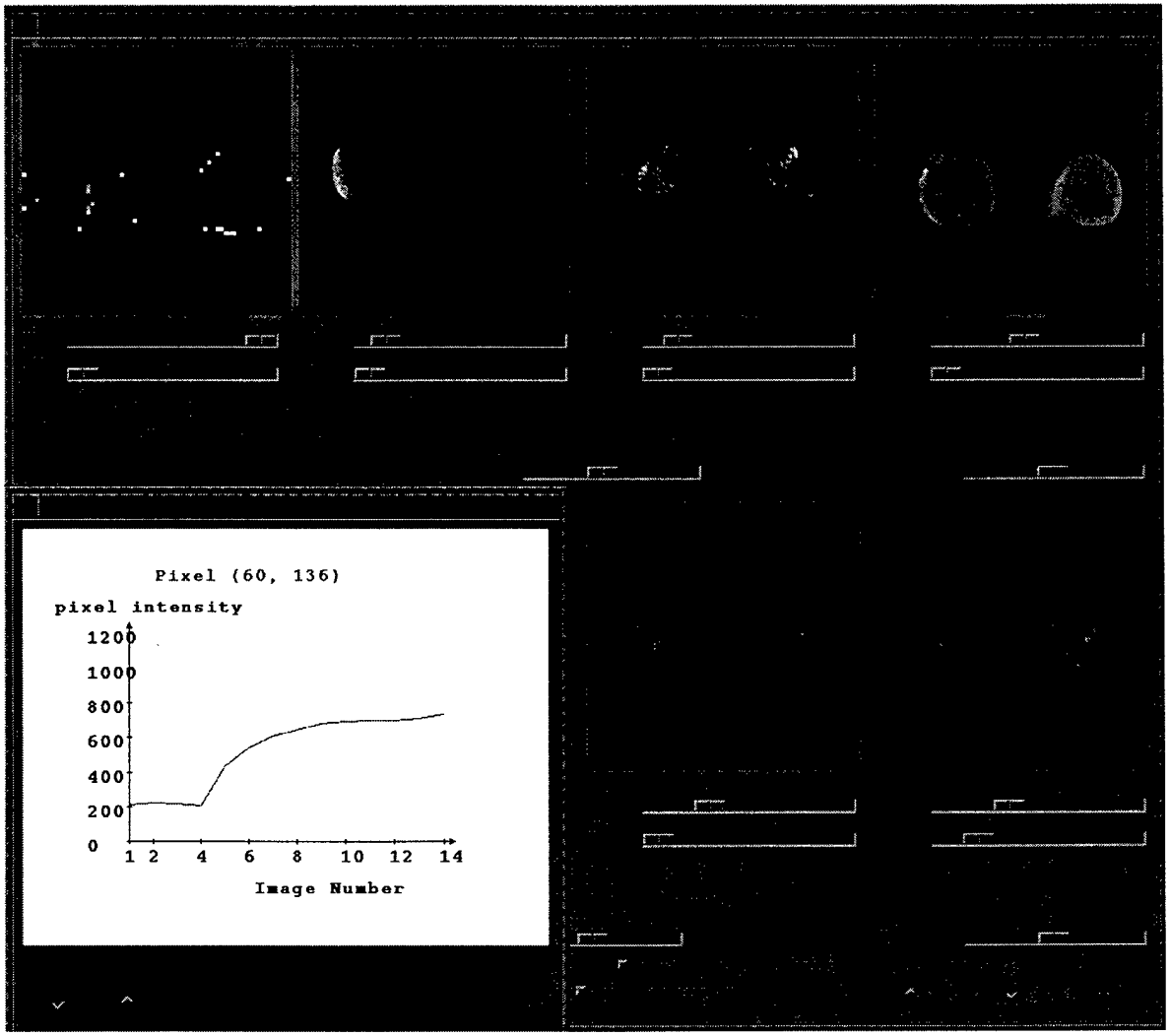

Figure 5. Aug 7, 1998 breast study. Time series of signal changes at a rapidly enhancing pixel during dynamic contrast enhancement. Also shown: T_1 feature image (1st from left), pre_contrast 3D image (2nd from left), post-contrast 3D image, last image of dynamic study, T_2 image, and max first derivative image.

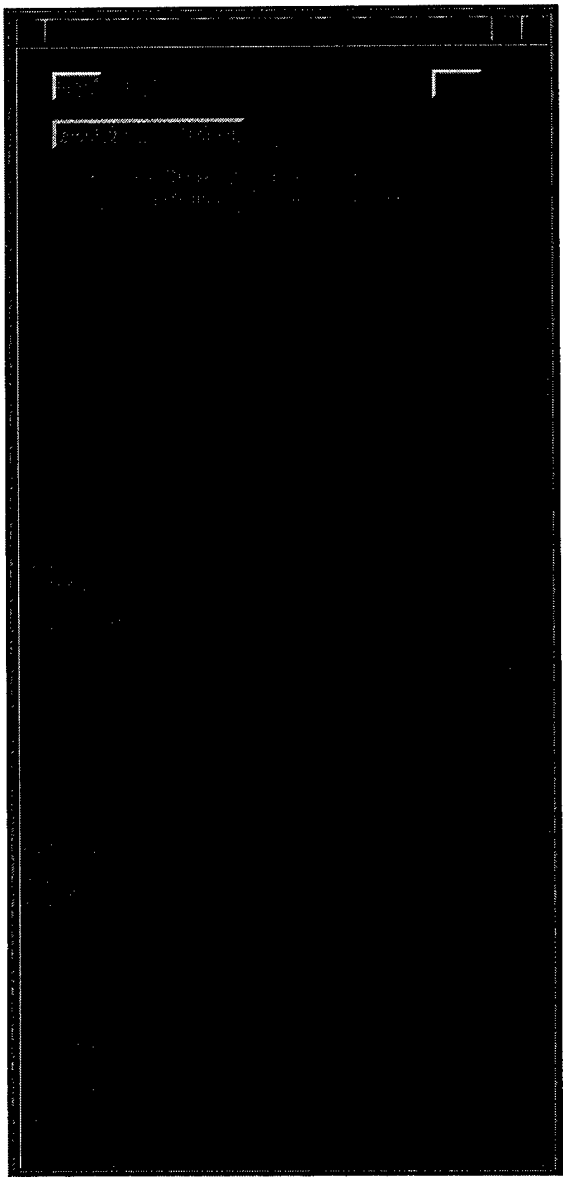

Figure 6. The opening page of the BreastView program.

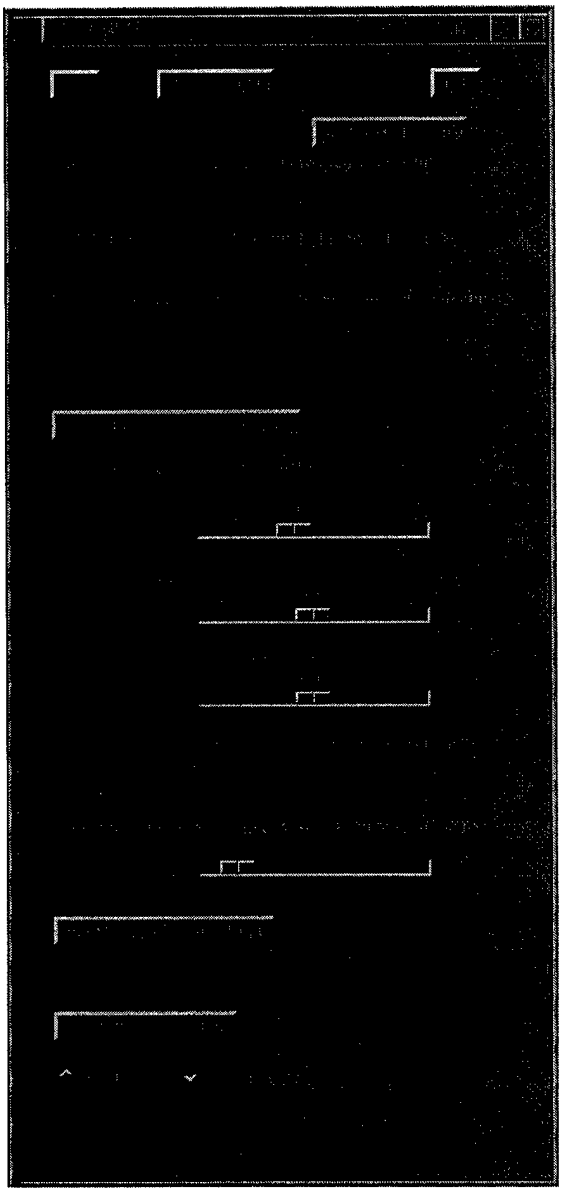

Figure 7. Aug 7, 1998 breast study. Suspicion level map is created using the "Create Detection Image" button after setting the thresholds.

Key Research Accomplishments

A. Pulse sequences that are compatible with a Signa Horizon LX EchoSpeed CV/i system, running LX 8.2.5 system software:

1. Fast SPGR-based arterial spin tagging sequence
2. Odd-number interleaved EPI sequence
3. Interleaved EPI-based arterial spin tagging sequence

B. Imaging processing software

1. BreastView
2. DispAlls
3. Bayesian analysis of arterial spin tagged image data

Reportable Outcomes

A. Pulse sequences for Version 8.2.5 (MH Buonocore and D Zhu):

1. Arterial spin tagging sequence with Fast SPGR Acquisition
2. Odd-number interleaf EPI
3. Arterial spin tagging sequence with Odd-number interleaf EPI acquisition
4. Arterial Spin Tagging sequence with Even-number hybrid EPI acquisition

B. Breast Imaging Protocols (MH Buonocore and D Zhu)

1. Anatomical, spin tagged, and dynamic c-e breast imaging protocol

C. SGI Graphics Software for Breast image analysis (MH Buonocore and D Zhu):

1. BreastView (display program for breast imaging protocol)
2. DispAll (display program for general MRI images)

D. PhD Degree in Biomedical Engineering, December 1999 (D Zhu)

E. Employment as GE Applications Engineer, starting Jan 2000 (D Zhu):

Conclusions

We have successfully converted and enhanced the arterial spin tagging pulse sequences to work on a new research MRI system, and have made several enhancements. Understanding of the 8.2.5 pulse sequence language on the new system represents a major advance of the project. These pulse sequences will be used in all future work, and hopefully there will not be a substantial MRI system upgrade such as we experienced for a few years at least. Image display and statistical analysis software has been written for the spin tagging and contrast enhanced studies, and to allow analysis to be done by a busy clinician without computer expertise.

References

1. Buonocore MH, Zhu DC. High spatial resolution EPI using an odd number of interleaves. Magnetic Resonance in Medicine 41 (6): 1199-1205 (1999).

2. Buonocore MH, Zhu DC, Zulim RA. Analysis software for breast imaging studies. Proceedings of the International Society for Magnetic Resonance in Medicine, 7th Annual Meeting and Exhibition, 3: 2172 (1999).

Appendices

Copy of publication, Buonocore MH, Zhu DC. High spatial resolution EPI using an odd number of interleaves. Magnetic Resonance in Medicine 41 (6): 1199-1205 (1999). **(pages 51-57)**

Magnetic Resonance in Medicine 41:1199–1205 (1999)

High Spatial Resolution EPI Using an Odd Number of Interleaves

Michael H. Buonocore* and David C. Zhu

Ghost artifacts in echoplanar imaging (EPI) arise from phase errors caused by differences in eddy currents and gradient ramping during left-to-right traversal of k_x (forward echo) versus right-to-left traversal of k_x (reverse echo). Reference scans do not always reduce the artifact and may make image quality worse. To eliminate the need for reference scans, a ghost artifact reduction technique based on image phase correction was developed, in which phase errors are directly estimated from images reconstructed separately using only the forward or only the reverse echos. In practice, this technique is applicable only to single-shot EPI that produces only one ghost (shifted ½ the field of view from the parent image), because the technique requires that the ghosts do not completely overlap the parent image. For higher spatial resolution, typically an even number of separate k-space traversals (interleaves) are combined to produce one large data set. In this paper, we show that data obtained from an even number of interleaves cannot be combined to produce only one ghost, and image phase correction cannot be applied. We then show that data obtained from an odd number of interleaves can be combined to produce only one ghost, and image phase correction can be applied to reduce ghost intensity significantly. This "odd-number interleaf EPI" provides spatial and temporal resolution tradeoffs that are complementary to, or can replace, those of even-number interleaf EPI. Odd-number interleaf EPI may be particularly useful for MR systems in which reference scans have been unreliable. Magn Reson Med 41:1199–1205, 1999.

Key words: magnetic resonance imaging; interleaved echo planar imaging; ghost artifact suppression; image phase correction

To increase spatial resolution in echoplanar imaging (EPI), two or more separate k-space traversals (interleaves) can be used to acquire different sets of k-space lines that are combined to produce one large data set. Typically, this "interleaved EPI" uses an even number of interleaves (1–4). Interleaved EPI is particularly sensitive to the generation of ghost artifacts, which arise from the differences in eddy currents and gradient ramping that occur during left-to-right traversal of k_x (forward echo, denoted *l*) versus right-to-left traversal of k_x (reverse echo, denoted *r*). These forward and reverse echos cause different phase errors that result, upon two-dimensional (2D) Fourier transformation, in ghost artifacts in the phase encode (k_y) direction. These ghosts can often be reduced using phase error information obtained from non-k_y encoded reference scans (5–11).

Previously, one of the authors published a ghost artifact reduction technique (12) based on extracting the spatially dependent phase errors directly from images reconstructed separately using only the forward or only the reverse echos. This technique was developed only for single-shot EPI, in which forward and reverse echos are alternated in k-space, and Fourier reconstruction produces a single ghost artifact shifted by ½ the field of view (FOV) from the location of the "parent" image. The technique requires, for each location in the frequency encode direction, at least one pixel within the parent image that the ghost artifact does not overlap. The technique could not be applied to even-number interleaf EPI that have been presented in the literature, because the multiple ghost artifacts produced in these scans entirely overlapped the parent image. With h interleaves, ghost and parent images were separated by only $\pm 1/2h$ the FOV.

This paper introduces and illustrates the advantages of using an *odd* number of interleaves. The fundamental criteria for the interleaved EPI sequence design was to achieve a k-space trajectory that mimics the following features of a single-shot EPI method that are critical to producing images without ghost artifacts: 1) smooth T2* decay of the signal as a function of k_y; and 2) phase errors due to forward and reverse echos arranged in an alternating *l-r-l-r-l-r-l-r-etc.* pattern as a function of k_y. Reduction of ghost artifacts from T_2^* decay has been previously addressed in the literature (2). In single-shot EPI, the decay is smooth as a function of k_y and causes only a local blurring of the image. In interleaved EPI, the decay can significantly affect image quality if the combined data set is strongly modulated as a function of k_y. Strong modulation is avoided by temporally delaying each interleaf in accordance with its starting k_y, such that the combined data set acquires a smooth T_2^* decay in the k_y direction. As we will show, the need to assemble a *l-r-l-r-l-r-l-r-etc.* alternation of phase errors in the interleaved EPI data set leads naturally to the use of an odd-number of interleaves. An odd number is necessary to generate a single ghost that is well separated from the parent image and to utilize image phase correction.

THEORY

Let N equal the number of raw data points in the k_x and k_y directions and in the final image. Define $g_{lr}(n)$ according to the direction of the nth k-space line,

$$g_{lr}(n) = \begin{cases} 1 & \text{if } n\text{th line acquired from left to right (forward echo)} \\ -1 & \text{if } n\text{th line acquired from right to left (reverse echo)} \end{cases} \quad [1]$$

and define $\theta(x, y)$ as the phase errors at each echo center (with forward and reverse echos differing in the sign of θ),

Department of Radiology, UC Davis Medical Center, Sacramento, California.

Presented in part at the 6th Annual Meeting of the International Society of Magnetic Resonance in Medicine, April 17–25, 1998, Sydney, Australia.

*Correspondence to: Michael H. Buonocore, Dept. of Radiology, TICON-II, 2nd floor, UC Davis Medical Center, Sacramento, CA 95817.

Received 18 May 1998; revised 21 December 1998; accepted 19 January 1999.

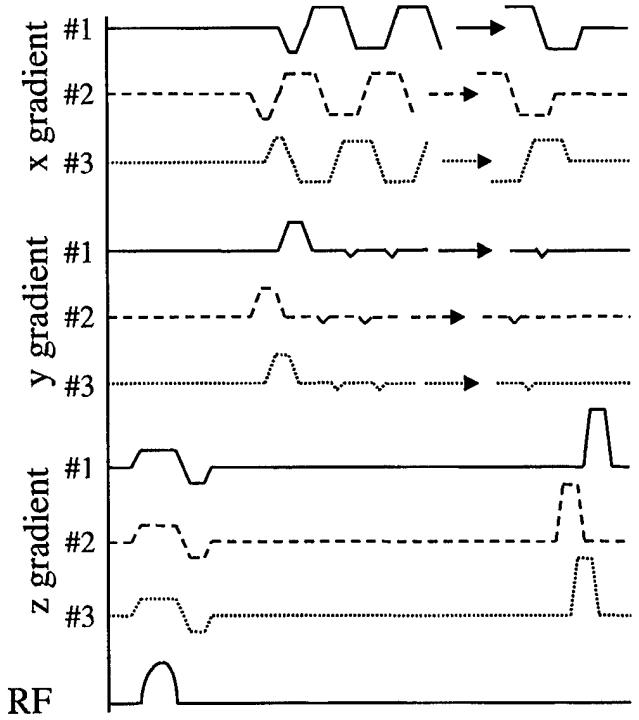

FIG. 1. Three-interleaf EPI pulse sequence diagram. For each interleaf, relative temporal delays and polarity changes of x (frequency encode), y (phase encode), and z (slice-select) gradient waveforms are shown for each of the three interleaves (labeled #1, #2, and #3). Interleaf #1 acquires the 1st k-space line and every third thereafter. Interleaves #2 and #3 acquire the 2nd and 3rd k-space lines and every third line thereafter, but the first acquired k-space line from each interleaf is discarded. To create a smooth T2* decay in the combined data set, interleaves #2 and #3 are temporally shifted such that their 2nd acquired k-space line is offset by 1/3 and 2/3 of the total time for one trapezoid of the readout gradient. Phase encoding occurs at the transitions between forward and reverse echos and is also temporally shifted in each interleaf. The slice-select gradient has a constant spoiler gradient after data acquisition to reduce residual transverse magnetization. Z-gradient and RF pulses for slice selection are identical for all interleaves.

due to gradient-dependent main field offsets, echo delays, and echo drifts. If the data alternate between forward and reverse echos in successive k-space lines, then $g_{lr}(n) = 1$ for n even, and $g_{lr}(n) = -1$ for n odd. This alternating pattern of echos produces a single ghost shifted ½ the FOV, which can be suppressed using image phase correction (12).

Multiple ghost artifacts, some shifted only a small distance from the parent image, occur with more complicated patterns of forward and reverse echos as a function of k_y. To derive the relation between the echo pattern, and the locations and complex amplitude factors of resulting ghosts, define

$$g_l(n) = \tfrac{1}{2}(1 + g_{lr}(n)) \quad \text{and} \quad g_r(n) = \tfrac{1}{2}(1 - g_{lr}(n)) \quad [2]$$

as functions identifying, respectively, the forward and reverse echos as a function of k-space line indexed by n. Set the spatial scale such that the object being reconstructed, $M(x,y)$, is defined at $N \times N$ integer-valued points (x, y) in the spatial domain. Following from Eq. [3] in ref. 12, the signal at points labeled by integers in k-space can then be written as

$$S(m, n) = (1/N^2) \sum_{x=-N/2}^{N/2-1} \sum_{y=-N/2}^{N/2-1} M(x, y) \times (g_l(n) \exp(i\theta(x, y)) + g_r(n) \exp(-i\theta(x, y))) \cdot \exp\left(-i\frac{2\pi}{N} mx\right) \exp\left(-i\frac{2\pi}{N} ny\right) \quad [3]$$

Regrouping terms, and carrying out an Inverse Fourier transform on Eq. [3], the reconstructed image, $M(x, y)$, can

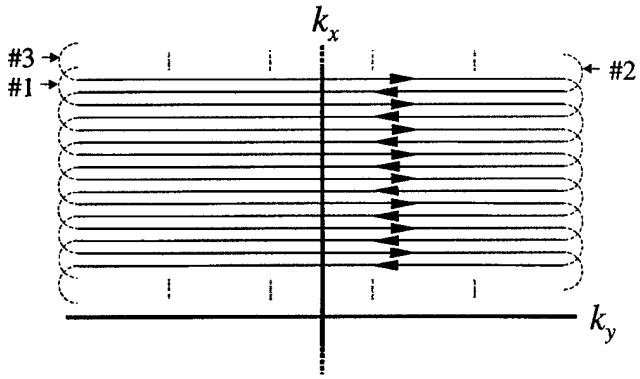

FIG. 2. Odd-number interleaf EPI. Three separate interleaves (labeled #1, #2, and #3) are combined to produce a *l-r-l-r-l-r-l-r-etc.* pattern of echos. In our implementation of 128 × 128 interleaved EPI, each interleaf acquires 44 k-space lines, yielding an excess of 4 lines that are discarded. Interleaf #1 acquires the 1st, 4th, 7th, etc. k-space lines (counting from 1 at top), interleaf #2 acquires the 2nd, 5th, 8th, etc. lines, and interleaf #3 acquires the 3rd, 6th, 9th, etc. lines. Interleaves #1 and #2 are initiated with a forward echo, while interleaf #3 is initiated with a reverse echo. The first acquired k-space line from interleaf #2, and the first acquired line from interleaf #3, are not used in the combined data set. Also, the last k-space line (131th in combined data set) from interleaf #3, and the last line from interleaf #1 (132th in combined data set) are discarded. Discarding the first k-space lines is based on the presumption that equilibrium phase errors may occur only after the first line, meaning that the 2nd and 3rd lines of the combined data set should not be acquired as the 1st line of one of the interleaves.

Table 1
Interleaved EPI Used for Figs. 4–7

No. of interleaves	Data matrix of each interleaf[1]	Resulting image matrix[1]
1	64 × 64	64 × 64
2	128 × 64	128 × 128
3	128 × 44	128 × 128
9	256 × 30	256 × 256

[1]Matrices are given as frequency encode × phase encode.

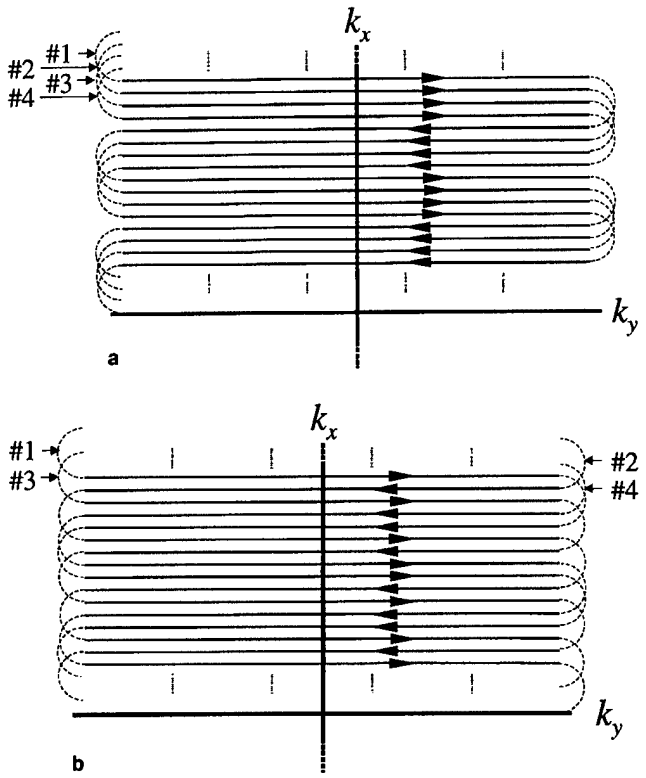

FIG. 3. Even-number interleaf EPI. In our implementation of 128 × 128 interleaved EPI, each interleaf acquires 32 k-space lines, and no lines are discarded. Four separate interleaves (labeled #1, #2, #3, and #4) are combined to produce different echo patterns. Each figure shows exactly two cycles of the smallest repeating pattern of the combined data set. **a:** A *l-l-l-l-r-r-r-r-etc.* pattern is formed by using interleaf #j (j = 1, 2, 3, or 4) to acquire the j^{th}, $(j + 4)^{th}$, $(j + 8)^{th}$, $(j + 12)^{th}$, etc. k-space lines. Each interleaf is initiated with a forward echo. **b:** A *l-r-l-r-r-l-r-l-etc.* pattern is formed by acquiring the same lines with each interleaf as in a, but initiating interleaves #2 and #4 each with a reverse echo. Locations and relative intensities of ghost artifacts from these patterns are computed using Eq. [8] with $h = 4$, and are listed in Table 2.

be written

$$\hat{M}(x, y) = M(x, y) \cos(\theta(x, y)) + \sum_{y'=-N/2}^{N/2-1} M(x, y') G_{lr}(y - y') \sin(\theta(x, y')) \quad [4]$$

where, similar to that in ref. 13, $G_{lr}(y - y')$ is defined as the Ghost Kernel given by

$$G_{lr}(y - y') \equiv (i/N) \sum_{n=-N/2}^{N/2-1} g_{lr}(n) \exp\left(-i \frac{2\pi}{N} n (y - y')\right) \quad [5]$$

Based solely on the periodicity of g_{lr} with n, the Ghost Kernel can also be written

$$G_{lr}(y - y') \equiv \sum_{j=-h}^{h-1} g_j \delta(y - y' - \Delta_j) \quad [6]$$

where $\Delta_j = N/2hj$, $j = -h+1, \ldots, h-1$, and δ a delta-like function defined by

$$\delta(y) \equiv (1/N) \sum_{n=-N/1}^{N/2-1} \exp\left(-i \frac{2\pi}{N} ny\right) = \begin{cases} 1 & \text{if } y = 0 \text{ Modulo } N \\ 0 & y \text{ integer} \neq 0 \end{cases} \quad [7]$$

Eq. [6] explicitly identifies each ghost location Δ_j and complex amplitude factor g_j. Substitution of Eq. [7] into Eq. [6], and comparison with Eq. [5], reveals the Fourier Transform relationship between $g_{lr}(n)$ and g_j:

$$g_{lr}(n) = -i \sum_{j=-h}^{h-1} g_j \exp\left(i \frac{2\pi}{N} n\Delta_j\right)$$
$$g_j = (i/2h) \sum_{n=-h}^{h-1} g_{lr}(n) \exp\left(-i \frac{2\pi}{N} n\Delta_j\right) \quad [8]$$

These equations show that the maximum number of ghosts is equal to $2h$, and the separation between the parent image and the two nearest (most-overlapping) ghosts are $\Delta_1 = N/2h$ and $\Delta_{-1} = -N/2h$ or $\pm 1/2h$ the FOV.

MATERIALS AND METHODS

Interleaved gradient-recalled EPI was implemented on a Signa Advantage 1.5 T MR System (GE Medical Systems,

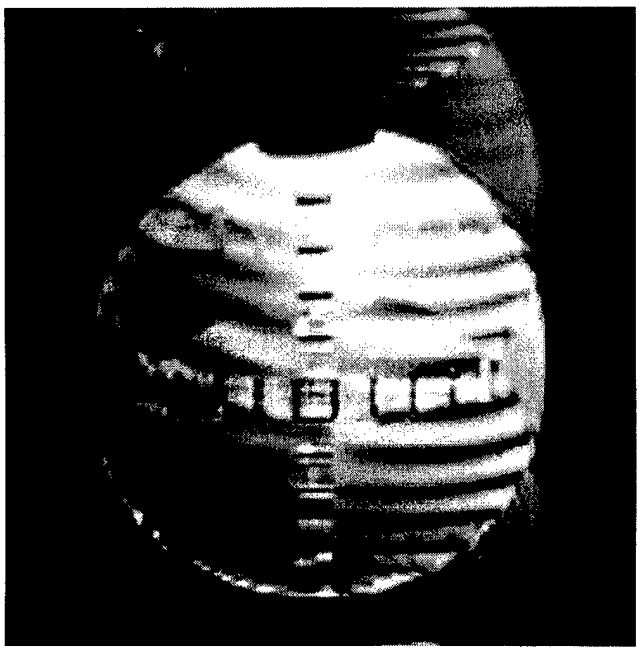

FIG. 4. Image of phantom using even-number interleaf EPI. In this implementation of 128 × 128 interleaved EPI, each of two interleaves acquired 64 k-space lines, and no lines were discarded. A *l-l-r-r-l-l-r-r-etc.* pattern of echos was formed by using interleaf #j (j = 1 or 2) to acquire the j^{th}, $(j + 2)^{th}$, $(j + 4)^{th}$, etc. k-space lines. Each interleaf was initiated with a forward echo. Locations and relative intensities of ghost artifacts in the image can be computed using Eq. [8] with $h = 2$. The locations Δ_j and complex amplitude factors g_j for these ghosts, denoted $(\Delta_j/N, g_j)$, (with $N = 128$ image matrix size) are $(-\frac{1}{2}, 0)$, $(-\frac{1}{4}, \frac{1}{2}i - \frac{1}{2})$, $(\frac{1}{4}, \frac{1}{2}i + \frac{1}{2})$. These parameters are used in Eq. [4] to describe the image.

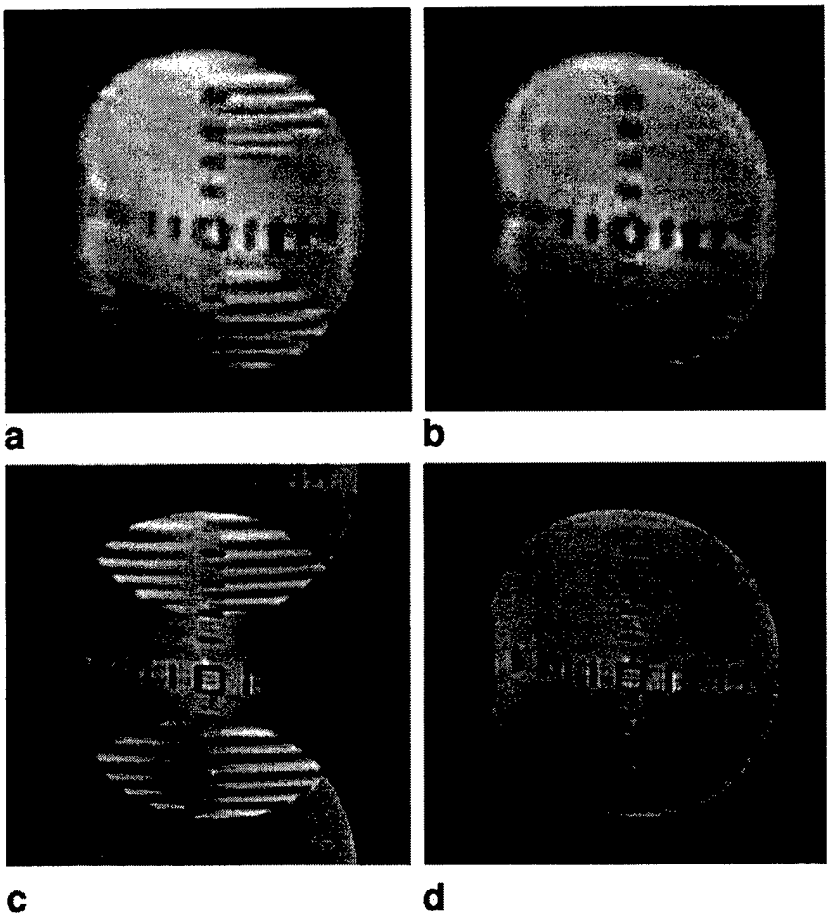

FIG. 5. Axial images of phantom obtained from single-shot and odd-number interleaf EPI, with and without ghost artifact reduction using image phase correction. **a:** 64 × 64 single-shot EPI with *l-r-l-r-l-r-l-r-etc.* pattern of echos. **b:** Image phase correction reduces average ghost intensity to 2.3% of average parent image intensity. **c:** 128 × 128 three-interleaf EPI, implementation described in text to generate *l-r-l-r-l-r-l-r-etc.* pattern of echos. **d:** Image phase correction reduces average ghost intensity to 4.3% of average parent image intensity.

Waukasha, WI) with Version 5.4 Genesis software platform. An insertable three-axis gradient and radiofrequency (RF) coil set (Medical Advances, Milwaukee, WI) was used, providing 2.0 g/cm peak gradient strength and 56 μsec rise time, and permitting 64×64 single-shot acquisitions in under 40 msec per image, and with duty cycle permitting up to 9 images/sec. Figure 1 shows the pulse sequence diagram for three interleaf EPI.

Specific interleaved EPI scans were performed on phantoms and normal subjects. Informed consent was obtained from all subjects. The following parameters were common to all scans: TE 40 msec, flip angle 90°, FOV 220 mm, slice thickness 6 mm, slice gap 2 mm, and number of locations 16. Phantom studies were run with TR 3.2 sec and subject studies with TR 2 sec. Table 1 shows the different interleaved scans that were performed and the resulting image matrix sizes. All images were linearly interpolated to 256 × 256 for display. After image phase correction, residual ghost intensity was measured as the average intensity of the image in the entire ghost-only region of the image, divided by the average intensity in the entire parent-only region of the image, and reported as a percentage.

RESULTS

Predictions of Theory

Typical interleaved EPI data sets assembled with forward and reverse echos grouped together produce ghosts that significantly overlap the parent image. Because image phase correction requires at least a one-pixel wide strip within the parent image that does not contain ghost, the technique cannot be applied with any such interleaved data sets (unless the FOVs were made impracticably large to separate the adjacent ghosts). However, if the interleaved EPI data could be arranged to have purely alternating forward and reverse echos (i.e., *l-r-l-r-l-r-l-r-etc.* pattern), then the resulting uncorrected reconstruction would have only one ghost shifted by ½ the FOV, and image phase correction could be applied.

Odd-Number Interleaf EPI

Even-number interleaf EPI cannot produce the required alternating pattern, but odd-number interleaf EPI can. The three interleaf EPI echo pattern is shown in Fig. 2. For comparison, two different even-number interleaf EPI echo patterns are shown in Fig. 3. Figure 3a shows a *l-l-l-l-r-r-r-r-etc.* pattern resulting from identical traversals of k-space of four interleaves. Figure 3b shows a *l-r-l-r-r-l-r-l-etc.* pattern resulting from alternating the direction of the traversal of interleaves #2 and #4. More detailed consideration reveals that the simple *l-r-l-r-l-r-l-r-etc.* pattern cannot be obtained from an even number of interleaves.

Experimental Verification

Figure 4 shows a 128 × 128 image obtained using two interleaf EPI (composed of two 128 × 64 interleaves). There are two ghosts shifted by ±¼ of the FOV, arising from the *l-l-r-r-l-l-r-r- etc.* pattern of phase errors. The ghost

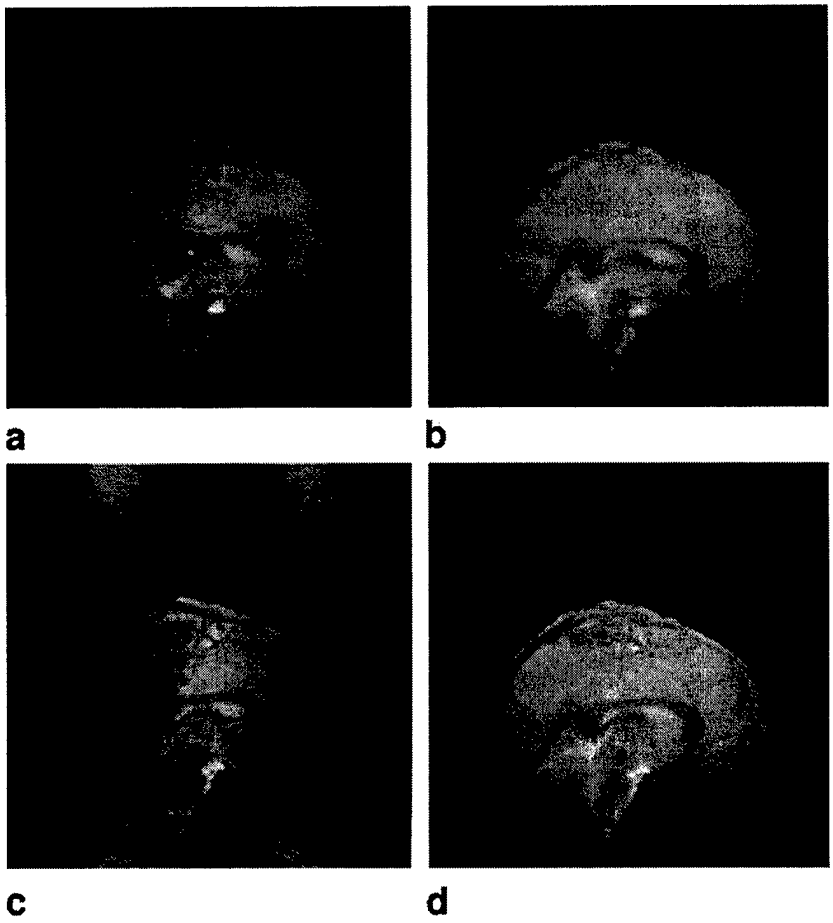

FIG. 6. Sagittal images of head obtained from single-shot and odd-number interleaf EPI, with and without ghost artifact reduction using image phase correction. **a:** 64 × 64 single-shot EPI with *l-r-l-r-l-r-l-r-etc.* pattern of echos. **b:** Image phase correction reduces average ghost intensity to 1.6% of average parent image intensity. **c:** 128 × 128 three-interleaf EPI, implementation described in text to generate *l-r-l-r-l-r-l-r-etc.* pattern of echos. **d:** Image phase correction reduces average ghost intensity to 5.6% of average parent image intensity.

shifted by ½ the FOV has zero amplitude. Ghost artifact reduction by image phase correction is not possible, because the parent image is almost everywhere overlapping with ghost. Figure 5a shows an image from 64 × 64 single-shot EPI, and Fig. 5b shows removal of the N/2 ghost using image phase correction. Figure 5c shows an image from 128 × 128 odd-number interleaf EPI composed of three 128 × 44 interleaves and confirms that the sequence causes only a single ghost shifted by ½ the FOV. Figure 5d confirms that image phase correction largely suppresses this ghost. Figure 6 displays similar results obtained in the sagittal plane on a normal subject. Figure 6a shows an image from 64 × 64 single-shot EPI with a single ghost artifact, and Fig. 6b shows removal of the ghost using image phase correction. Figure 6c shows an image from 128 × 128 odd-number interleaf EPI composed of three 128 × 44 interleaves, and confirms that the sequence causes only a single ghost shifted by ½ the FOV. Figure 6d confirms that image phase correction largely suppresses this ghost. Figure 7 shows images from 256 × 256 odd-number interleaf EPI (composed of nine 256 × 30 interleaves). These images confirm that large odd-number interleaf EPI produces only a single ghost shifted by ½ the FOV.

Comparison of Even- and Odd-Number Interleaf EPI

Table 3 lists possible desired image resolutions and compares data acquisition time, number of slices, and temporal

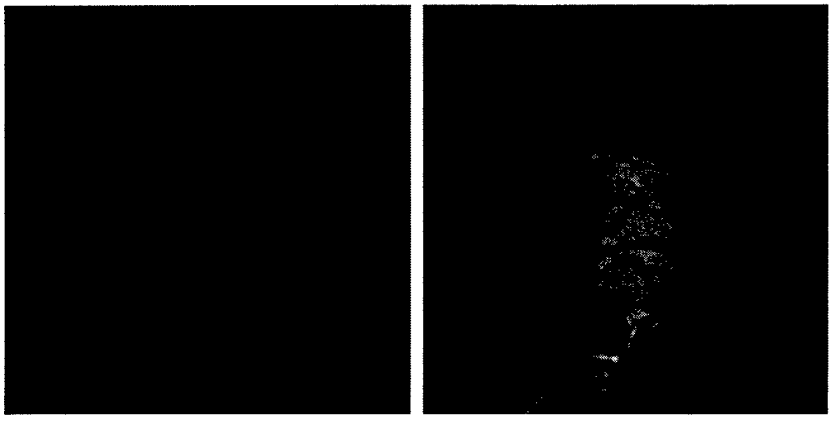

FIG. 7. Axial phantom (left) and sagittal head (right) images obtained from odd-number interleaf EPI. 256 × 256 combined data set with *l-r-l-r-l-r-l-r-etc.* pattern of echos was acquired using nine 256 × 30 interleaves. Interleaf #j, j = 1,2, ..., 9, was used to acquire the j^{th}, $(j + 9)^{th}$, $(j + 18)^{th}$, $(j + 27)^{th}$ k-space line (number from 1 starting at top), and interleaves #3, #5, #7, and #9 were initiated with reverse echos (all others were initiated with forward echos). The first acquired k-space lines were discarded in interleaves #2 through #9, as were the last acquired lines in interleaves #1, #5 through #9. The lack of ghosts, other than that shifted by ½ the FOV, validates the assumption that phase errors represented by $\pm\theta(x)$ are the same in separately acquired interleaves.

Table 2
Ghost Complex Amplitude Factors in $h = 4$ Interleaved EPI Shown in Fig. 3*

Ghost location offset	*l-l-l-l-r-r-r-r-*etc. pattern	*l-r-l-r-r-l-r-l-*etc. pattern
−½	0	0
−⅜	$0.25\,i - 0.10$	$0.25\,i + 0.60$
−¼	0	0
−⅛	$0.25\,i - 0.60$	$0.25\,i + 0.10$
0	0	0
⅛	$0.25\,i + 0.60$	$0.25\,i - 0.10$
¼	0	0
⅜	$0.25\,i + 0.10$	$0.25\,i - 0.60$

*Ghost position offsets are Δ_j, $j = -h, -h+1, \ldots, h-1$, as defined in Eq. [6], and are listed here as fractions of the FOV and relative to the location of parent image. Ghost complex amplitude factors are g_j, as defined in Eqs. [6] and [8]. The echo pattern repeats across the phase encode direction, and the amplitude factors are calculated assuming that the first letter of the pattern gives the direction at $k_y = 0$. Note that both patterns generate ghosts close to the parent image at $\pm 1/2h = \pm$⅛ the FOV.

resolution that can be obtained using odd number versus even-number interleaf EPI. The table entries are computed with fMRI neural activation experiments in mind, in which temporal resolution of not worse than 3000 msec would typically be required. For a given spatial resolution and number of interleaves, the right two columns give the number of distinct slice locations that can be obtained (constrained by 3000 msec temporal resolution), and the required TR (defined as the time interval between acquisition of sequential interleaves at a given slice). The table reveals that odd-number interleaf EPI is complementary to even-number interleaf EPI, and one may argue that either set alone would be sufficient for the vast majority of fMRI experiments.

DISCUSSION

Based on our experience, reference scans are not as reliable as image phase correction (12). Not infrequently, poor reference scans make the image quality worse by virtue of poor estimation of the phase errors in the image data. Reference scans will be proportionally more unreliable in interleaved EPI when separate phase corrections are required for each interleaf. A recent comparison (14) between image reference correction with two established reference scan methods (5,11) showed that image phase correction reduced artifact more.

If the user is willing to increase the acquisition time, then the problem of overlapping ghost artifact can be avoided by either 1) doubling the FOV while maintaining

Table 3
Comparison of Even- and Odd-Number Interleaf EPI

Data matrix (freq × ph)	No. of leafs	k-lines/ leaf	Time/leaf (ms)	k-lines acquired	k-lines discarded	No. of slices with 3000 ms temporal resolution	Required TR (ms) for 3000 ms temporal resolution
64 × 64	1	64	39.9	64	0	27	3000
128 × 128	2	64	72.7	128	0	7	1500
128 × 128	3	44	50.0	132	4	7	1000
128 × 128	4	43	36.4	128	0	7	750
128 × 128	5	27	30.7	135	7	7	600
192 × 128	3	44	72.5	132	4	4	1000
192 × 128	4	32	52.7	128	0	5	750
192 × 128	5	27	44.5	135	7	4	600
192 × 128	6	23	37.9	138	10	4	500
192 × 192	4	48	79.1	192	0	3	750
192 × 192	5	40	65.9	200	8	3	600
192 × 192	6	32	52.7	192	0	3	500
192 × 192	7	29	47.8	203	11	3	428
256 × 192	6	32	69.1	192	0	2	500
256 × 192	7	29	62.6	203	11	2	428
256 × 192	8	24	51.8	192	0	2	375
256 × 192	9	23	49.7	207	15	2	333
256 × 128	4	32	69.1	128	0	3	750
256 × 128	5	27	58.3	135	7	3	600
256 × 128	6	23	49.7	138	10	3	500
256 × 128	7	20	43.2	140	12	3	428
256 × 256	8	32	69.1	256	0	1	375
256 × 256	9	30	64.8	270	14	1	333
256 × 256	10	27	58.3	270	14	1	300
256 × 256	11	25	54.0	275	19	1	272

Table lists only those acquisitions producing 30 ms < time/leaf < 80 ms. Headings: Time/leaf: computed using 8 us sampling rate and 56 us gradient rise time. Data matrix: combined raw data array size, freq: frequency encode direction, ph: phase encode direction; k-lines discarded: Excess k-space lines not needed for reconstruction; No. of slices . . . : Estimated from time/leaf and duty cycle limit: of local gradient coil (LGC); Required TR (ms) . . . : TR needed to acquire combined data set.

the pixel size by doubling the number of phase encode steps; 2) retaining the FOV and acquiring lines only in one direction with an asymmetric gradient waveform as in ABEST (15,16); or 3) doubling the number of phase encode steps using a standard readout waveform and performing two reconstructions, first using only the forward lines and then only the reverse lines, with image averaging to improve the signal-to-noise ratio (e.g., ref. 17). The odd-number interleaf EPI is valuable because in most EPI applications it is an optimal strategy to match the FOV to the object size and minimize the number of phase encode steps, to make image acquisition as rapid and with as few interleaves as possible, while avoiding image wraparound. This strategy reduces artifacts from physiological motion and maximizes temporal resolution for imaging dynamical processes.

REFERENCES

1. McKinnon GC. Ultrafast interleaved gradient echo planar imaging on a standard scanner. Magn Reson Med 1993;30:609–616.
2. Butts K, Riederer SJ, Ehman RL, Thompson RM, Jack CR. Interleaved echo planar imaging on a standard MRI system. Magn Reson Med 1994;31:67–72.
3. Feinberg DA, Oshio K. Phase errors in multi-shot echo planar imaging. Magn Reson Med 1994;32:535–539.
4. Slavin GS, Butts K, Rydberg JN, Jack CR, Riederer SJ. Dual-echo interleaved echo-planar imaging of the brain. Magn Reson Med 1995;33: 264–270.
5. Bruder H, Fischer H, Reinfelder HE, Schmitt F. Image reconstruction for echo planar imaging with nonequidistant k-space sampling. Magn Reson Med 1992;23:311–323.
6. Wong EC. Shim insensitive phase correction for EPI using a two echo reference scan. In: Proceedings of the SMRM, 11th Annual Meeting, Berlin, Germany, 1992. p 4514.
7. Jesmanowicz A, Wong EC, Hyde JS. Phase correction for EPI using internal reference lines. In: Proceedings of the SMRM, 12th Annual Meeting, New York, 1993. p 1239.
8. Maier JK, Vevrek M, Glover GH. Correction of NMR data acquired by an echo planar technique. US Patent #5,151,656 (1992).
9. Jesmanowicz A, Wong EC, Hyde JS. Self-correcting EPI reconstruction algorithm. In Proceedings of the SMR, 3rd Annual Meeting, Nice, France, 1995. p 619.
10. Mandeville JB, Weisskoff RM, Garrido L. Reduction of eddy-current induced Nyquist ghosts and sampling artifact. In: Proceedings of the SMR, 3rd Annual Meeting, Nice, France, 1995. p 613.
11. Hu X, Le TH. Artifact reduction in EPI with phase encoded reference scan. Magn Reson Med 1996;36:166–176.
12. Buonocore MH, Gao L. Ghost artifact reduction for echo-planar imaging using image phase correction. Magn Reson Med 1997;38:89–100.
13. Reeder SB, Atalar E, Bolster BD, McVeigh ER. Quantification and reduction of ghosting artifacts in interleaved echo-planar imaging. Magn Reson Med 1997;38:429–439.
14. Clare S, Bowtell R, Morris P. Ghost artefact in fMRI: comparison of techniques for reducing the N/2 ghost. In: Proceedings of the ISMRM, on CD-ROM. 1998. p 2137.
15. Feinberg DA, Turner R, Jakab PE, von Kienlin M. Echo-planar imaging with asymmetric gradient modulation and inner-volume excitation. Magn Reson Med 1990;13:162–169.
16. Hennel F, Nedelec J-F. Interleaved asymmetric echo-planar imaging. Magn Reson Med 1995;34:520–524.
17. Posse S, Tedeschi G, Risinger R, Ogg R, Le Bihan D. High speed ^{1}H spectroscopic imaging in human brain by echo planar spatial-spectral encoding. Magn Reson Med 1995;33:34–40.